

Bayesian Random Semantic Data Augmentation for Medical Image Classification

Yaoyao Zhu^{1,2}[0009-0008-4943-608X], Xiuding Cai^{1,2}[0000-0002-2038-7164],
Xueyao Wang^{1,2}[0009-0002-3304-4993], and Yu Yao^{1,2}[0000-0003-4752-0102]

¹ Chengdu Institute of Computer Application, Chinese Academy of Sciences,
Chengdu, China

² University of Chinese Academic Sciences, Beijing, China
{zhuyaoyao19,caixiuding20,wangxueyao221}@mails.ucas.ac.cn,casitmed2022@163.com

Abstract. Data augmentation is a critical regularization technique for deep neural networks, particularly in medical image classification. Popular data augmentation approaches include image transformation-based methods, generative data augmentation, and automatic data augmentation. However, these approaches encounter notable limitations: image transformation-based and automated data augmentation techniques cannot implement semantic transformations, leading to a constrained variety of augmented samples, and generative data augmentation methods are computationally expensive. In response to these challenges, we proposed *Bayesian Random Semantic Data Augmentation* (BRSDA), a novel, efficient, and plug-and-play semantic data augmentation method. BRSDA is motivated by a simple translation in the feature space along specific directions that can effectuate semantic transformations. When given a feature, we define its augmentable semantic magnitude as a random variable and estimate its distribution using variational Bayesian, then sample semantic magnitude and add to the randomly selected semantic direction to achieve semantic data augmentation. We demonstrate the effectiveness of BRSDA on five 2D and six 3D medical image datasets covering nine modalities. We also test BRSDA with mainstream neural network architectures, showcasing its robustness. Furthermore, combining BRSDA with other leading data augmentation methods achieves superior performance. Code is available online at <https://github.com/YaoyaoZhu19/BRSDA>.

Keywords: Data Augmentation · Medical Image · Variational Bayesian.

1 Introduction

Data augmentation is a common regularization technique used to address the overfitting problem during the training process of deep neural networks, widely applied in medical image classification [15,23]. Although methods based on image transformations (such as cropping, mirroring, rotation, and color jittering) and automatic data augmentation methods (such as AA [4], RA [5], etc.) can increase the diversity of the dataset to some extent, they mainly achieve this

through simple geometric or pixel-level transformations, limiting their ability to perform complex semantic transformations [25]. Generative data augmentation methods [8,22], especially those based on Generative Adversarial Networks [3,12] or diffusion models [17,19], offer a powerful solution capable of performing complex semantic transformations and significantly increasing data diversity, such as changing images’ background or foreground textures. However, generative methods are computationally expensive and inconvenient to use.

Recent works have underscored the enhanced efficacy of data augmentation when applied within the feature space [2,10,13,24]. In detail, the deep feature space harbors various semantic directions, and shift features along these directions yields new sample features with identical class identities but alter semantic content [25]. The ISDA [25] stands out in this domain, facilitating implicit data augmentation by aiming to minimize an upper bound of the expected cross-entropy loss on the augmented dataset. Unlike traditional methods that modify images directly, this approach generated new data at the feature level, such as operating random disturbances, interpolations, or extrapolations within the feature space for augmentation [6]. In medical images, there are numerous modalities with non-uniform dimensions. The computational cost of generative data augmentation methods is high. However, the effectiveness of techniques based on image transformation could be more satisfactory. Semantic data augmentation holds promise in addressing the shortcomings of both approaches. To our knowledge, there is currently no published literature on semantic data augmentation methods within medical image classification.

To develop a universal semantic augmentation paradigm for medical image classification, we drew inspiration from the automatic augmentation method: RA [5], defining a semantic data augmentation strategy incorporating two hyperparameters: semantic magnitude and semantic direction. Inspired by the concept that modeling data augmentation as additive perturbation can enhance network learning and generalization capabilities [14], we define a semantic data augmentation method as the addition of semantic magnitude to the original feature in randomly selected semantic direction. For example, in the tumor staging task, a feature represents the semantics of tumor size, and we change the tumor size by changing the feature value. However, alterations beyond the permissible range within the category may result in label changes. Therefore, we treat the augmentable (label-preserving) semantic magnitude as a random variable and estimate its distribution using variational Bayesian. For semantic directions, similar to the image space augmentation approach [7], it is a naive idea to select semantic directions randomly, but it does not make sense to perform augmentation in certain directions [25], a view based on image space. Some data augmentation approaches [8,28] are adequate for downstream tasks, although they do not make sense vision, and the quantitative evaluation approaches proposed in [27] explain why vision meaningless data augmentation approaches are still practical. Not coincidentally, [13] point out that adding a random Gaussian perturbation to the features significantly improves the Empirical Risk Minimization (ERM), although it does not follow any meaningful direction. Even the perturbation of

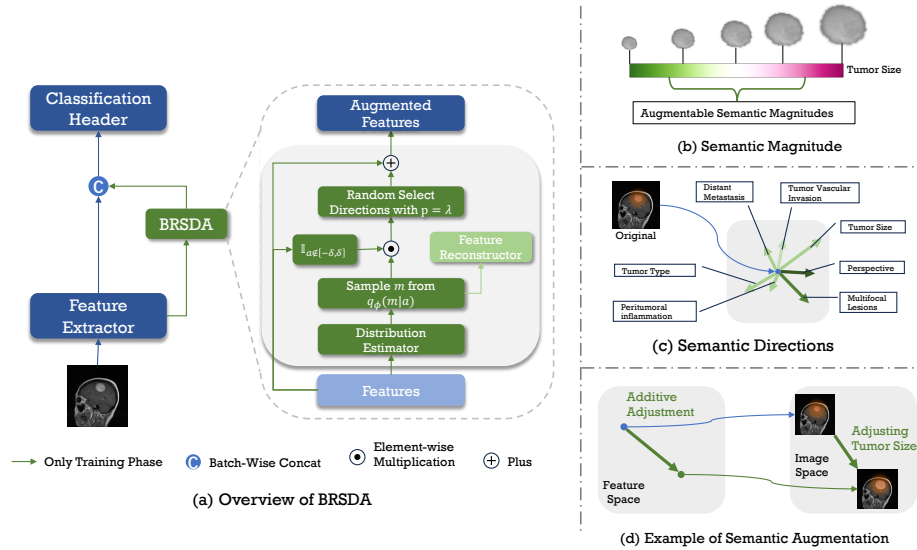


Fig. 1. (a) Overview of our proposed method. The figure illustrates the BRSDA as a plug-in into the networks. The dashed box in the figure shows the steps of BRSDA. (b) Example of augmentable semantic magnitude. (c) Examples of different semantic directions in feature space. (d) Examples of semantic data augmentation corresponding to semantic changes in image space. (b), (c) and (d) are not shown explicitly.

randomness due to the reparameterization introduced by variational inference benefits the network’s learning of features [13]. Therefore, we do not augment all directions but randomly select semantic directions like the random selection transform in image space. We proposed Bayesian Random Semantic Data Augmentation (BRSDA), a method for deep neural network training in medical image classification. BRSDA generates new data by sampling semantic magnitude from augmentable semantic magnitude distribution, randomly choosing semantic directions, and adding magnitude to the original feature. Figure 1 illustrates the BRSDA approaches. Our main contributions are listed below:

1. We propose a high-performance, plug-and-play Bayesian random semantic data augmentation module, BRSDA, for medical image classification.
2. BRSDA improves network performance in medical image classification tasks with different dimensions, modalities, and neural network architectures.
3. We provide experiments that show BRSDA can significantly elevate network performance in conjunction with other data augmentation methods.

2 Method

Considering training a deep neural network $G_\theta = f_1 \circ f_2$ included two parts: a feature extraction network f_1 and a classification network f_2 with parameters θ

on a dataset $\mathcal{D} = \{(\mathbf{x}_i, \mathbf{y}_i)\}_{i=1}^N$, where each \mathbf{y}_i represents a label belonging to one of c classes. The output of f_1 is a k dimensions feature vector $\mathbf{a} = f_1(\mathbf{x}) \in \mathcal{R}^k$, which is then input into f_2 to predict the target $\hat{\mathbf{y}} = f_2(\mathbf{a}) = f_2(f_1(\mathbf{x}))$, where $\hat{\mathbf{y}}$ is the predicted class label. We refer to \mathbf{a} as the original feature vector for clarity.

BRSDA The BRSDA method generates augmented feature $\tilde{\mathbf{a}}$ by adding the semantic magnitude \mathbf{m} to the original feature \mathbf{a} after element-wise multiplication of them with randomly selected semantic directions \mathbf{d}_λ . The formula is as follows:

$$\tilde{\mathbf{a}} = \mathbf{a} + \mathbf{d}_\lambda \odot \mathbf{m}, \quad (1)$$

where $\mathbf{d} \in \{0, 1\}^k$ is a binary vector, initially set to all ones and then set to zero with probability λ . $\mathbf{m} \in \mathcal{R}^k$ represents the semantic magnitude sampled from the augmentable magnitude distribution $p(\mathbf{m}|\mathbf{a})$ when given the original feature vector \mathbf{a} . Furthermore, to preserve specific properties of the features, such as low rank, we mask semantic directions corresponding to zero feature values. We have:

$$\tilde{\mathbf{a}} = \mathbf{a} + \mathbb{I}_{\mathbf{a} \neq 0} \mathbf{d}_\lambda \odot \mathbf{m}, \quad (2)$$

where $\mathbb{I}_{\mathbf{a} \neq 0}$ is an indicator function when $\mathbf{a} \neq 0$, the value of this function is 1.

Estimate the magnitude distribution To obtain $p(\mathbf{m}|\mathbf{a})$, we introduce a model $q_{\phi_{\mathbf{m}}}(\mathbf{m}|\mathbf{a})$ to approximate the true distribution $p(\mathbf{m}|\mathbf{a})$. The Kullback-Leibler (KL) divergence measures the similarity between these two distributions, aiming to make $q_{\phi_{\mathbf{m}}}(\mathbf{m}|\mathbf{a})$ closely match $p(\mathbf{m}|\mathbf{a})$ by maximizing the KL divergence. Thus, our optimization goal is as follows:

$$\tilde{\phi}_{\mathbf{m}} = \arg \max_{\phi_{\mathbf{m}}} D_{KL}(q_{\phi_{\mathbf{m}}}(\mathbf{m}|\mathbf{a}) || p(\mathbf{m}|\mathbf{a})). \quad (3)$$

Removing the terms that are not related to the parameter $\tilde{\phi}_{\mathbf{m}}$ in D_{KL} , we have:

$$D_{KL}(q_{\phi_{\mathbf{m}}}(\mathbf{m}|\mathbf{a}) || p(\mathbf{m}|\mathbf{a})) = \text{KL}(q_{\phi_{\mathbf{m}}}(\mathbf{m}|\mathbf{a}) || p(\mathbf{m})) - \mathbb{E}_{\mathbf{m} \sim q_{\phi_{\mathbf{m}}}(\mathbf{m}|\mathbf{a})}(\log p(\mathbf{a}|\mathbf{m})). \quad (4)$$

The loss of BRSDA The first term of Eq. 4 can be calculated easily. The second term estimates the features \mathbf{a} given \mathbf{m} , which is more challenging to compute. Drawing inspiration from the design of Variational Autoencoders (VAE) [11], we introduce a reconstruction network for learning this term, rewriting the second term as $p_{\phi_{\mathbf{a}}}(\mathbf{a}|\mathbf{m})$. Then, we obtain the loss function of BRSDA as follows:

$$\mathcal{L}_{brsda}(\phi_{\mathbf{m}}, \phi_{\mathbf{a}}; \mathbf{a}) = -\text{KL}(q_{\phi_{\mathbf{m}}}(\mathbf{m}|\mathbf{a}) || p(\mathbf{m})) + \mathbb{E}_{\mathbf{m} \sim q_{\phi_{\mathbf{m}}}(\mathbf{m}|\mathbf{a})}(\log p_{\phi_{\mathbf{a}}}(\mathbf{a}|\mathbf{m})). \quad (5)$$

The second part of Eq. 5 depends on the model, and we use MSE loss in BRSDA. Assuming the marginal distribution $p(\mathbf{m})$ follows a normal distribution $\mathcal{N}(0, \mathbf{I})$

and $q_{\phi_{\mathbf{m}}}(\mathbf{m}|\mathbf{a})$ also follows a normal distribution $\mathcal{N}(0, \sigma^2)$, setting the mean to zero because we aim to learn the offset relative to the original rather than the augmented feature. Thus, the loss function of BRSDA is given by:

$$\mathcal{L}_{brsda}(\phi_{\mathbf{m}}, \phi_{\mathbf{a}}; \mathbf{a}) = -\frac{1}{2} \sum_{i=0}^N (1 + \log(\sigma^2) - \sigma^2) + \frac{1}{2N} \sum_{l=1}^N (\hat{\mathbf{a}} - \mathbf{a})^2, \quad (6)$$

where σ^2 is estimated variance of BRSDA, and $\hat{\mathbf{a}}$ is reconstructed feature using \mathbf{m} .

Relationship with VAE Our approach resembles VAE [11], where a latent variable is estimated and used for reconstruction. However, the relationship between our latent variable \mathbf{m} and the inputs differs from VAE [11], the latent variable representation of the inputs in VAE [11]. Our latent variable \mathbf{m} represents the augmentable range in a given feature \mathbf{a} without altering the label.

The reparameterization trick We employ the reparameterization trick to facilitate the computation of the loss function while ensuring the gradient flow for effective backpropagation. The random variable \mathbf{m} can be represented as a deterministic variable $\mathbf{m} = g_{\phi_{\mathbf{m}}}(\epsilon, \mathbf{a})$, with $\epsilon \sim \mathcal{N}(0, \mathbf{I})$ being an auxiliary variable with an independent marginal distribution $p(\epsilon)$, and $g_{\phi_{\mathbf{m}}}$ being a vector-valued function parameterized by $\phi_{\mathbf{m}}$.

Loss function Our augmentation method is training with G_{Θ} . For convenience, we denote the loss of G_{Θ} as \mathcal{L}_{task} , which typically uses cross-entropy loss in classification tasks. Therefore, the total loss function is:

$$\mathcal{L} = \mathcal{L}_{task}^{\mathbf{a}} + \alpha(\mathcal{L}_{brsda} + \mathcal{L}_{task}^{\hat{\mathbf{a}}}). \quad (7)$$

Different superscripts on \mathcal{L}_{task} distinguish between augmented and original features. The hyperparameter α is a dynamic value introduced to mitigate the impact of BRSDA on the network during the initial stages of training when the network has yet to learn valuable features.

In summary, the BRSDA method can be plugged into deep networks. We present the pseudo-code of BRSDA in Algorithm 1.

3 Experiments

Our evaluation strategy encompassed several vital aspects: effectiveness across modalities and dimensions, adaptability to convolutional neural networks, and comparison and combination with non-semantic data augmentation methods. Area under ROC curve (AUC) and Accuracy (ACC) are used as the evaluation metrics. Moreover, we report the results of the parameters ablation study, parameter sensitivity tests, and feature visualization in Appendix A.

Algorithm 1 The BRSDA algorithm

Input: \mathcal{D}
 Randomly initialize Θ , $\phi_{\mathbf{a}}$, and $\phi_{\mathbf{m}}$
for $t = 0$ to T **do**
 Sample a mini-batch $\{\mathbf{x}_i, \mathbf{y}_i\}_{i=1}^B$ from \mathcal{D}
 Compute features $\mathbf{a}_i = G(\mathbf{x}_i)$
 Estimate variance of magnitude distribution σ_i
 Compute *magnitudes* \mathbf{m}_i using reparameterization trick $\mathbf{m}_i = \sigma_i \odot \epsilon_i$
 Compute *augmented features* $\tilde{\mathbf{a}}_i$ according to Eq. 2
 Compute reconstructed features $\hat{\mathbf{a}}_i$
 Compute \mathcal{L} according to Eq.(7)
 Update Θ , $\phi_{\mathbf{a}}$, and $\phi_{\mathbf{m}}$
end for

3.1 Datasets and Training Details

Dataset We chose publicly available five 2D medical image datasets (BreastMNIST [26], RetinaMNIST [26], BTMRI [18], LUNG [20], and CATAR [1]) and six 3D medical image datasets from the MedMNISTv2 [26] pository in our evaluation. Further details about these datasets can be found in Table 1.

Training Details We implemented BRSDA using PyTorch and experimented on an NVIDIA RTX 4090 GPU. During training, we utilized the AdamW [16] optimizer with a learning rate of 0.001, resized all 2D images to 224×224 and 3D images to $64 \times 64 \times 64$, and we employed a learning rate warm-up for the first five epochs followed by a cosine annealing learning rate decay strategy. To ensure fairness, we maintain consistent training configurations across all experiments. The distribution estimator and reconstruction modules of BRSDA comprise two fully connected layers followed by BatchNorm and GeLU activation. Additional details about hyperparameters of networks and BRSDA can be found in Appendix B.

3.2 Results

Results of dataset Table 1 demonstrates that BRSDA improves the AUC of the model in all cases. For instance, when the network is equipped with the BRSDA module, AUC and accuracy increase on the BreastMNIST [26] dataset. BRSDA also performs excellently on 3D datasets, such as SynapseMNIST3D [26], increasing AUC and accuracy. On the other hand, for datasets like BTMRI [18], CATAR [1], and OrganMNIST3D [26], the improvement appears marginal. The baseline results were already high, and further gains were limited. In the case of BTMRI and NoduleMNIST3D, we observed an adverse change in accuracy. It happens because the dataset is not perfectly balanced. Meanwhile, AUC is unaffected by the decision threshold, while ACC is affected by the threshold.

Table 1. Performance of different datasets on the test set using ResNet-18 [7]. The best results are **bold-faced**, while the number in brackets denotes the performance improvements achieved by BRSDA compared with the Baseline. 'Baseline' represents the results without any data augmentation, and 'BRSDA' indicates the results with the addition of our method. Modality in the last column of the dataset. The dataset with 3D inside the name are 3D images, and the others are 2D images.

Dataset	AUC%		ACC%		Modality
	Baseline	BRSDA	Baseline	BRSDA	
BreastMNIST [26]	89.62	92.13 _(2.51)	84.62	87.82 _(3.21)	Breast Ultrasound
RetinaMNIST [26]	71.69	72.60 _(0.91)	45.00	52.50 _(7.50)	Fundus Camera
LUNG [20]	87.48	89.05 _(1.58)	77.31	78.72 _(1.42)	X-Ray
BTMRI [18]	99.81	99.93 _(0.12)	97.64	97.48 _(-0.15)	MRI
CATAR [1]	97.98	98.88 _(0.90)	89.26	92.56 _(3.31)	Camera
OrganMNIST3D [26]	99.35	99.38 _(0.04)	89.02	89.51 _(0.49)	CT
NoduleMNIST3D [26]	89.65	91.31 _(1.66)	87.42	85.81 _(-1.61)	CT
AdernalMNIST3D [26]	88.60	89.13 _(0.54)	71.81	83.89 _(12.08)	Shape from CT
FractureMNIST3D [26]	74.09	77.17 _(3.09)	52.50	52.50 _(0.00)	CT
VesselMNIST3D [26]	95.79	96.47 _(0.68)	94.50	94.50 _(0.00)	Shape from MRI
SynapseMNIST3D [26]	71.18	76.06 _(4.89)	75.00	76.99 _(1.99)	Electron Microscope

Results of network architectures In Table 2, we report the results of testing on the BreastMNIST [26] dataset using mainstream deep convolutional neural network architectures. BRSDA enhances the performance across various network architectures. Notably, Adding the BRSDA module to baseline EfficientNet-B0 improves performance. This improvement might be attributed to overfitting during the training of the baseline EfficientNet-B0. After all, its performance was lower than the baseline of the other networks. Therefore, BRSDA helps mitigate overfitting and provides evidence that BRSDA is a regularization technique. The cost of all improvement is an increase in training time of less than 4%. The results for ResNet-18 [7] are better than those for ResNet-50 [7], which aligns with the results reported in the original MedMNISTv2 [26] paper.

Result of methods Table 3 displays the experimental results of BRSDA and ISDA combining other data augmentation methods. The results of BRSDA (third row) and ISDA (second row) experiments suggest that semantic data augmentation methods can enhance non-semantic data augmentation techniques in most situations, collectively aiding networks in learning better features. Interestingly, in the experiments based on Random Augmentation (RA), the addition of semantic data augmentation leads to a decline in results, but combining ISDA and BRSDA can increase the AUC of the model. Table 3 demonstrates that combining BRSDA and ISDA can complement both deficiencies to achieve better results. The last row shows that the AUC metric performs best when training with three methods (ISDA, BRSDA, and non-semantic data augmentation

Table 2. Evaluation of BRSDA on different convolutional neural networks using the test set of BreastMNIST [26]. The best results are **bold-faced**, while the number in brackets denotes the performance improvements achieved by BRSDA. The last column is about the additional time introduced by BRSDA.

Network	AUC %		ACC %		Additional Time %
	Baseline	BRSDA	Baseline	BRSDA	
ResNet-18 [7]	89.62	92.13 _(2.51)	84.62	87.82 _(3.21)	1.75
ResNet-50 [7]	87.16	87.99 _(0.84)	81.41	83.33 _(1.92)	3.02
EfficientNet-B0 [21]	76.46	85.29 _(8.82)	80.13	82.69 _(2.56)	3.22
DenseNet-121 [9]	89.95	92.31 _(2.36)	85.90	87.18 _(1.28)	1.73

Table 3. Evaluation of BRSDA with State-Of-The-Art data augmentation methods on the test set of LUNG [20] dataset using ResNet-18 [7](Baseline AUC=87.48% and ACC=77.31%). The best results are **bold-faced** and underlined remarked second one. 'MA,' 'RA,' 'AA' and 'AM' refer to MedAugment [15], RandAugment [5], AutoAugment [4] and AugMix [8] are non-semantic data augmentation methods. We report the results of different semantic data augmentation methods trained with non-semantic data augmentation methods. The last row combines ISDA [25] and BRSDA methods.

Method	AUC %				ACC %			
	MA	RA	AA	AM	MA	RA	AA	AM
Baseline	92.20	<u>94.07</u>	89.25	87.61	78.01	84.40	82.98	75.18
ISDA [25]	<u>93.26</u>	92.91	90.10	91.48	81.56	<u>81.56</u>	76.60	<u>82.27</u>
BRSDA	93.03	93.06	<u>91.76</u>	91.94	85.11	78.01	<u>81.56</u>	83.69
ISDA+BRSDA	94.30	94.46	92.24	<u>91.51</u>	<u>83.69</u>	80.14	<u>81.56</u>	81.56

methods). As with Table 1, AUC increases, but ACC decreases for the same reason.

4 Conclusion

This paper introduces an efficient, plug-and-play Bayesian Random Semantic Data Augmentation (BRSDA) method for medical image classification. BRSDA generates new samples in feature space, which will be more efficient and easy to implement. We experimentally demonstrate the effectiveness and efficiency of BRSDA on different modalities, different dimensional datasets, and different networks. Furthermore, we show that integrating BRSDA with other data augmentation techniques, including ISDA, can significantly elevate model performance.

References

1. Cataract dataset. <https://www.kaggle.com/datasets/nandanp6/cataract-image-dataset> (2024), accessed: 2024-01-28

2. Ahn, E., Kumar, A., Fulham, M., Feng, D., Kim, J.: Unsupervised domain adaptation to classify medical images using zero-bias convolutional auto-encoders and context-based feature augmentation. *IEEE Transactions on Medical Imaging* **39**(7), 2385–2394 (2020). <https://doi.org/10.1109/TMI.2020.2971258>
3. Chai, L., Wang, Z., Chen, J., Zhang, G., Alsaadi, F.E., Alsaadi, F.E., Liu, Q.: Synthetic augmentation for semantic segmentation of class imbalanced biomedical images: A data pair generative adversarial network approach. *Computers in Biology and Medicine* **150**, 105985 (2022)
4. Cubuk, E.D., Zoph, B., Mané, D., Vasudevan, V., Le, Q.V.: Autoaugment: Learning augmentation strategies from data. In: 2019 IEEE/CVF Conference on Computer Vision and Pattern Recognition (CVPR). pp. 113–123 (2019). <https://doi.org/10.1109/CVPR.2019.00020>
5. Cubuk, E.D., Zoph, B., Shlens, J., Le, Q.V.: Randaugment: Practical automated data augmentation with a reduced search space. In: 2020 IEEE/CVF Conference on Computer Vision and Pattern Recognition Workshops (CVPRW). pp. 3008–3017 (2020). <https://doi.org/10.1109/CVPRW50498.2020.00359>
6. DeVries, T., Taylor, G.W.: Dataset augmentation in feature space. arXiv preprint arXiv:1702.05538 (2017)
7. He, K., Zhang, X., Ren, S., Sun, J.: Deep residual learning for image recognition. In: Proceedings of the IEEE conference on computer vision and pattern recognition. pp. 770–778 (2016)
8. Hendrycks, D., Mu, N., Cubuk, E.D., Zoph, B., Gilmer, J., Lakshminarayanan, B.: AugMix: A simple data processing method to improve robustness and uncertainty. Proceedings of the International Conference on Learning Representations (ICLR) (2020)
9. Huang, G., Liu, Z., Van Der Maaten, L., Weinberger, K.Q.: Densely connected convolutional networks. In: Proceedings of the IEEE conference on computer vision and pattern recognition. pp. 4700–4708 (2017)
10. Kang, Y., Zhao, X., Zhang, Y., Li, H., Wang, G., Cui, L., Xing, Y., Feng, J., Yang, L.: Improving domain generalization performance for medical image segmentation via random feature augmentation. *Methods* **218**, 149–157 (Oct 2023). <https://doi.org/10.1016/j.ymeth.2023.08.003>, <https://www.sciencedirect.com/science/article/pii/S1046202323001329>
11. Kingma, D.P., Welling, M.: Auto-encoding variational bayes. arXiv preprint arXiv:1312.6114 (2013)
12. Li, D., Yang, J., Kreis, K., Torralba, A., Fidler, S.: Semantic segmentation with generative models: Semi-supervised learning and strong out-of-domain generalization. In: Proceedings of the IEEE/CVF Conference on Computer Vision and Pattern Recognition. pp. 8300–8311 (2021)
13. Li, P., Li, D., Li, W., Gong, S., Fu, Y., Hospedales, T.M.: A simple feature augmentation for domain generalization. In: 2021 IEEE/CVF International Conference on Computer Vision (ICCV). pp. 8866–8875 (2021). <https://doi.org/10.1109/ICCV48922.2021.00876>
14. Liu, T.Y., Mirzsoleiman, B.: Data-efficient augmentation for training neural networks. In: Koyejo, S., Mohamed, S., Agarwal, A., Belgrave, D., Cho, K., Oh, A. (eds.) *Advances in Neural Information Processing Systems*. vol. 35, pp. 5124–5136. Curran Associates, Inc. (2022), https://proceedings.neurips.cc/paper_files/paper/2022/file/2130b8a44e2e28e25dc7d0ee4eb6d9cf-Paper-Conference.pdf
15. Liu, Z., Lv, Q., Li, Y., Yang, Z., Shen, L.: Medaugment: Universal automatic data augmentation plug-in for medical image analysis. *ArXiv abs/2306.17466* (2023), <https://api.semanticscholar.org/CorpusID:259309293>

16. Loshchilov, I., Hutter, F.: Decoupled weight decay regularization. arXiv preprint arXiv:1711.05101 (2017)
17. Moghadam, P.A., Van Dalen, S., Martin, K.C., Lennerz, J., Yip, S., Farahani, H., Bashashati, A.: A morphology focused diffusion probabilistic model for synthesis of histopathology images. In: Proceedings of the IEEE/CVF Winter Conference on Applications of Computer Vision. pp. 2000–2009 (2023)
18. Nickparvar, M.: Brain tumor mri dataset (2021). <https://doi.org/10.34740/KAGGLE/DSV/2645886>, <https://www.kaggle.com/dsv/2645886>
19. Pinaya, W.H., Tudosiu, P.D., Dafflon, J., Da Costa, P.F., Fernandez, V., Nachev, P., Ourselin, S., Cardoso, M.J.: Brain imaging generation with latent diffusion models. In: MICCAI Workshop on Deep Generative Models. pp. 117–126. Springer (2022)
20. Tahir, A.M., Qiblawey, Y., Khandakar, A., Rahman, T., Khurshid, U., Musharavati, F., Islam, M., Kiranyaz, S., Al-Maadeed, S., Chowdhury, M.E.: Deep learning for reliable classification of covid-19, mers, and sars from chest x-ray images. *Cognitive Computation* pp. 1–21 (2022)
21. Tan, M., Le, Q.: Efficientnet: Rethinking model scaling for convolutional neural networks. In: International conference on machine learning. pp. 6105–6114. PMLR (2019)
22. Tran, T., Pham, T., Carneiro, G., Palmer, L., Reid, I.: A bayesian data augmentation approach for learning deep models. *Advances in neural information processing systems* **30** (2017)
23. Vu, Y.N.T., Wang, R., Balachandar, N., Liu, C., Ng, A.Y., Rajpurkar, P.: Medaug: Contrastive learning leveraging patient metadata improves representations for chest x-ray interpretation. In: Machine Learning for Healthcare Conference. pp. 755–769. PMLR (2021)
24. Wang, M., Yuan, J., Qian, Q., Wang, Z., Li, H.: Semantic data augmentation based distance metric learning for domain generalization. In: Proceedings of the 30th ACM International Conference on Multimedia. p. 3214–3223. MM '22, Association for Computing Machinery, New York, NY, USA (2022). <https://doi.org/10.1145/3503161.3547866>, <https://doi.org/10.1145/3503161.3547866>
25. Wang, Y., Huang, G., Song, S., Pan, X., Xia, Y., Wu, C.: Regularizing deep networks with semantic data augmentation. *IEEE Transactions on Pattern Analysis and Machine Intelligence* **44**(7), 3733–3748 (2022). <https://doi.org/10.1109/TPAMI.2021.3052951>
26. Yang, J., Shi, R., Wei, D., Liu, Z., Zhao, L., Ke, B., Pfister, H., Ni, B.: MedM-NIST v2 - A large-scale lightweight benchmark for 2D and 3D biomedical image classification. *Scientific Data* **10**(1), 41 (Jan 2023). <https://doi.org/10.1038/s41597-022-01721-8>, <https://doi.org/10.1038/s41597-022-01721-8>
27. Yang, S., Guo, S., Zhao, J., Shen, F.: Investigating the effectiveness of data augmentation from similarity and diversity: An empirical study. *Pattern Recognition* **148**, 110204 (2024)
28. Yun, S., Han, D., Chun, S., Oh, S.J., Yoo, Y., Choe, J.: Cutmix: Regularization strategy to train strong classifiers with localizable features. In: 2019 IEEE/CVF International Conference on Computer Vision (ICCV). pp. 6022–6031 (2019). <https://doi.org/10.1109/ICCV.2019.00612>

5 Appendix A

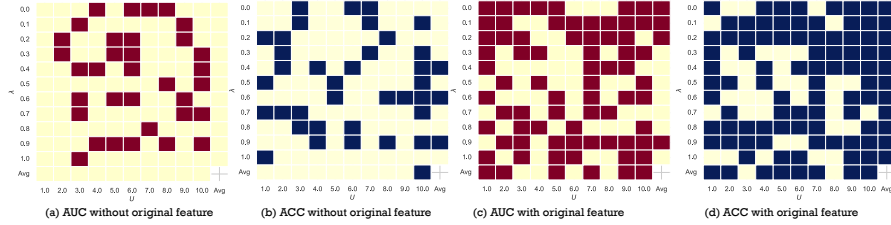


Fig. 2. Ablation study for BRSDA on BreastMNIST dataset using ResNet-18. Under the same hyper-parameters, if BRSDA improves performance relative to the baseline (AUC=89.62%, ACC=84.62%), the heatmap displays red(AUC) or blue(ACC). In each subplot, the horizontal axis represents the sampling rate U of BRSDA, while the vertical axis denotes the probability λ of random direction selection. (c) and (d) adds original features relative to (a) and (b).

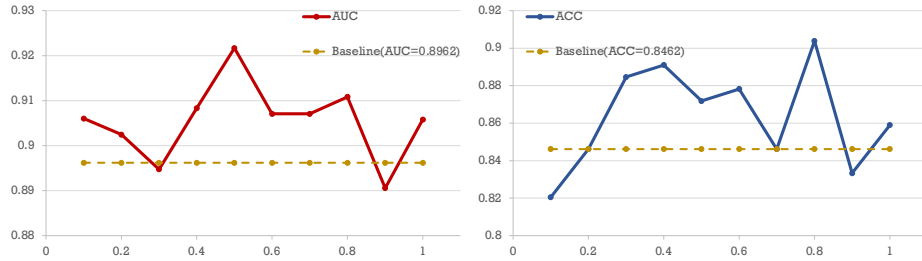


Fig. 3. Sensitivity analysis was conducted on the parameter λ of BRSDA using ResNet-18 on the BreastMNIST dataset. The horizontal axis indicates the values of λ , while the vertical axis illustrates the AUC and ACC performance metrics.

6 Appendix B

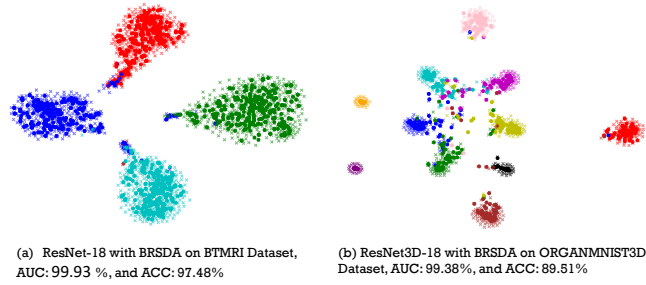


Fig. 4. Visualizing deep features using t-SNE, individual colors correspond to specific categories. Circular markers represent original features, while cross markers indicate augmented features generated by BRSDA.

Table 4. An Overview of Datasets.

Dataset	Modality	Tasks (Labels)	Samples	Train/Val/Test
BreastMNIST	Breast Ultrasound	Binary-Class (2)	780	546/78/156
RetinaMNIST	Fundus Camera	Ordinal Regression (5)	1,600	1,080/120/400
LUNG	X-Ray	Multi-Class (3)	701	419/141/141
BTMRI	MRI	Multi-Class (4)	7,023	4,568/1,144/1,311
CATAR	Camera	Multi-Class (2)	612	392/99/121
OrganMNIST3D	Abdominal CT	Multi-Class (11)	1,742	971/161/610
NoduleMNIST3D	Chest CT	Binary-Class (2)	1,633	1,158/165/310
AdrenalMNIST3D	Abdominal CT	Binary-Class (2)	1,584	1,188/98/298
FractureMNIST3D	Chest CT	Multi-Class (3)	1,370	1,027/103/240
VesselMNIST3D	Brain MRA	Binary-Class (2)	1,908	1,335/191/382
SynapseMNIST3D	Electron Microscope	Binary-Class (2)	1,759	1,230/177/352

Table 5. The setting of hyperparameters in experiments of BRSDA.

Dataset	Networks	Time %	λ	U	α	Explanation
BreastMNIST	ResNet-18	1.75	0.6	7	0.5	
BreastMNIST	ResNet-50	3.02	0.6	7	0.5	
BreastMNIST	EfficientNet-B0	3.22	0.6	7	0.5	
BreastMNIST	DenseNet-121	1.73	0.6	10	0.5	
RetinaMNIST	ResNet-18	2.06	0.6	10	0.5	
LUNG	ResNet-18	2.79	0.8	10	0.5	
BTMRI	ResNet-18	1.32	0.8	10	0.5	
CATAR	ResNet-18	0.59	0.9	10	0.5	
OrganMNIST3D	ResNet-18	-0.07	0.8	10	0.5	
NoduleMNIST3D	ResNet-18	0.14	0.9	10	0.5	
AdernalMNIST3D	ResNet-18	0.24	0.9	10	0.5	
FractureMNIST3D	ResNet-18	0.27	0.5	10	0.5	
VesselMNIST3D	ResNet-18	0.18	0.8	10	0.5	
SynapseMNIST3D	ResNet-18	0.51	0.4	10	0.5	
LUNG	ResNet-18	2.79	0.1	10	0.5	ISDA+BRSDA+MedAug
LUNG	ResNet-18	2.79	0.9	10	0.5	ISDA+BRSDA+RA
LUNG	ResNet-18	2.79	0.9	10	0.5	ISDA+BRSDA+AA
LUNG	ResNet-18	2.79	0.9	10	0.5	ISDA+BRSDA+AugMix